Multifunctional Ba(10-x) Nix La30 Si60 Glassy Composites for Thermoluminescent, and Opto-electronic Use

RK GUNTU (drgrk1985@gmail.com)

SNIST: Sreenidhi Institute of Science and Technology https://orcid.org/0000-0002-9842-4076

Research Article

Keywords: Barium lanthanum silicate glass, Elastic Studies, Photoluminescence, D.C. Conductivity, Thermoluminescence

Posted Date: August 24th, 2021

DOI: https://doi.org/10.21203/rs.3.rs-809562/v1

Multifunctional $Ba_{(10-x)}Ni_x La_{30} Si_{60}$ glassy composites for thermoluminescent, and opto-electronic use

Ravi Kumar Guntu

Department of Physics, Sreenidhi Institute of Science and Technology, JNT University, Hyderabad – 501 301, India.

Abstract

Past three decades to current literature, lanthanum silicates embedded with nickel ions are notable for different opto-electronic and semiconducting use. Current days of opto-electronics, including advanced semiconducting resources, need different assemblies of glass resources employing elastic, luminescent, and electronic characteristics. In this view, the opto-electronic resource of chemical composition $Ba_{(10-x)}Ni_xLa_{30}Si_{60}$ has planned for synthesis followed by mechanical, thermoluminescent, and opto-electronic characterization. The materials developed are showing glassy behavior, and which was confirmed by the structural characterization. The glass with 0.6 mol% NiO concentration exhibiting better thermal stability. Observations made on the elastic characterization of glasses suggested covalent structure. DTA results which include thermal stabilities of glasses, suggest materials are capable of high thermal stability. Molecular structure of glasses studied with the help of FT-IR spectra. Different structural units and their waves number positions are identified and analysed. Which also suggested glassy behavior. D.C. Conductivity reports suggest that the materials are electrically active, and they are showing few orders of ionic conductivity. A decrease in optical basicity with increasing NiO mol% of glasses suggests high order of covalence. Trap depth parameters (T_m, E_τ, E_δ, E_ω & μ_s) under thermoluminescence studies suggest glass with 0.6 mol% NiO concentration is a beneficial TL resource. Optical absorption spectra of glasses is recorded, and which helps to calculate the Racah parameters of glasses. Refractive index, emissive cross-section, optical band gap, and transition probability of nickel hosted present glasses evaluated with the help of photoluminescence characterization. This suggests glasses embedded with nickel ions are highly photonic. All the outcomes from the various characterization of glasses which include mechanical, thermoluminescent, and photo-electronic results, suggest a glass with 0.6 mol% NiO concentration is a helpful thermoelement and opto-electronic resource.

Keywords

Barium lanthanum silicate glass; Elastic Studies; Photoluminescence; D.C. Conductivity; Thermoluminescence;

Corresponding authors e-mail:

drgrk1985@gmail.com

I. INTRODUCTION

Naturally, SiO_2 glass materials are highly transparent, rigid, non-corrosive, and thermally stable. Their anticipated optical characteristics, such as high refractive index and optical bandgap, will be used for various optoelectronic industrial applications. Past three decades to current literature, there has been extensive investigation on silicate glass materials due to their abnormal optical results [1,2]. La_2O_3 is not a conventional glass former, but add-on La_2O_3 to the silicate glass materials improves their elastic nature, thermal stability, non-corrosion characteristics [3]. And also increase of La_2O_3 in the SiO_2 glass host lead to more microhardness and thermal stability. SiO_2 embedded with La_2O_3 glasses have a high order of thermally stimulated luminescence, which will highly

useful for radiation dosimetry processes [4]. The addition of BaO to the pure silicate host enhances the refractive index, reduces the glass discussion, and improves glass resource optically inert. Barium silicate glass materials embedded with transition metal oxides are the most favourable candidates in the current semiconducting sectors and finds plentiful usage in the area of photo-electronics [5]. La_2O_3 also influences SiO_2 ions to change the strength, chemical endurance, mechanical and spectroscopic properties to a considerable extent of the overall glass network [6]. BaO in silicate glass host stimulates nickel ions for better optical output. Metal oxide NiO is a good nucleation agent, which involves divalent oxidation states in silica glass matrix to enhance photo-electronic properties. Usually, Ni^{2+} ions have a substantial effect on the optical properties of glass materials. Silicate materials enclosing mixed valence states of Ni^{2+} ions are of recent interest as a cathode resource in rechargeable batteries as of their abnormal energy density and capacitance [7-9]. Subsequently, in the existing work, NiO doped lanthanum silicate materials were synthesized and report for their suitability regarding thermoluminescent photo-electronics. Potential functions such as abnormal elastic, thermoluminescent and photo-electric, etc., are achievable by improving tremendously advantageous solid-state glass materials that have captivated extensive attention [10]. Because of this, the current research aimed to prepare solid-state glass materials of chemical composition $(10\text{-}x)BaO+(x)NiO+30La_2O_3+60SiO_2$ and to study the $(BaO)_{(y-x)}(NiO)_x$ composite influence on opto-electronic, and TL characteristics of lanthanum silicate glasses.

II. METHOD, AND MEASUREMENTS

The chemicals of (10-x) mol% BaO, (x) mol% NiO, 30 mol% La_2O_3 and 60 mol% SiO_2 have been taken for sample preparation, where 'X varies with a step size 0.2 mol % from 0 to 1.0 mol %. The melt quenching technique is used to develop the present series of samples. Detailed chemical composition of the present series of glass tests are given as follows

ξ_0 10.0 BaO + 30 La_2O_3 + 60 SiO_2 + 0.0 NiO

ξ_2 09.8 BaO + 30 La_2O_3 + 60 SiO_2 + 0.2 NiO

ξ_4 09.6 BaO + 30 La_2O_3 + 60 SiO_2 + 0.4 NiO

ξ_6 09.4 BaO + 30 La_2O_3 + 60 SiO_2 + 0.6 NiO

ξ_8 09.2 BaO + 30 La_2O_3 + 60 SiO_2 + 0.8 NiO

ξ_{10} 09.0 BaO + 30 La_2O_3 + 60 SiO_2 + 1.0 NiO

Chemicals, SiO_2, La_2O_3, BaO, and NiO (Sigma Aldrich, AR grade 99 % pure) have been chosen in powder form. All the chemicals in suitable mol% were well mixed in an agate mortar. Programmed furnace and platinum crucibles were used to melt the chemical powder to form glass melt. Melting took place around at 1455 ^oC, observed, and quenched in the brass holder. Further, it was annealed around 500 ^oC as a glass. Dimensionally arranged glass samples were used for various characterization. Mass of the glasses recorded with the help of Scale Tech digital weighing balance with a precision of 10^{-4} gm/cm^3. Archimedes' principle was used to calculate the density values employing known weights of the glasses. Diffraction patterns of the glasses were recorded with the help of a Shimadzu X-ray (XRD 7000) diffractometer with a precision of 0.1 degrees. Chemical analysis was observed with the help of the Hitachi S 3700N instrument. And surface morphology of glasses was also recorded with a precision of $\pm$ 1 μm and within ~ 1 to 200 μm range. Ultrasonic velocities, which will be helpful to evaluate all elastic measurements of glasses, are recorded with the

help of a WT 311 D flaw detector with a precision of ± 10 m/s. FT IR Analysis was done with the help of Shimadzu 8400 S FT IR Spectrometer with a precision of ± 0.1 cm^{-1}. Thermal analyser Hitachi DTG-60 H is used to record the DTA Thermogram of glasses with a precision of ± 1 ºC. Thermoluminescence evaluations under gamma irradiation were recorded with the help of Nucleonix TL/OSL Reader with a precision of ± 1 ºC. Optical absorption spectra of glasses recorded with the help of V 670 Model, UV VIS NIR Spectrometer with a precision of 0.1 nm. Photoluminescence spectra of glasses recorded with the help of JASCO FP 6300 Spectrometer. DC Conductivity measurements are done by using Keithley 6514 Electrometer. MAT Lab 2.3, Chem Draw Ultra 12.0, and Mac Office 2013 plus software used to analyse the results.

III. RESULTS

Fig. 1 reports the X-ray diffraction recording of one of the glasses with 0.6 mol% NiO concentration. Experimental analysis suggests glassy behavior. Fig.2 reports chemical analysis of the glass with 0.6 mol% NiO concentration. Results obtained signify La, Ni, Si, O, and Ba with their atomic weight %. Physical properties of glasses are reported. The glass 'ξ_6' reported being best among all the values of various physical quantities of all series of glasses. All the results concerning the physical properties of the $Ba_{(10-x)}Ni_xLa_{30}Si_{60}$ glasses provide facts regarding the covalent structure of glasses. The following equations [11,12] are used to evaluate all the physical properties of glasses.

$$\text{Density of a glass } (D) = \{(S_a) / (S_a - S_w)\} \times D_{oxy}$$

$$\text{Molar Volume } (V_m) = M/D;$$

$$\text{Optical basicity } (\Lambda_{th}) = [(75) / (\xi - 1.35)];$$

Where, S_a - weight of a glass measured in air; S_{xy} - weight of glass measured in liquid ortho xylene;

D_{oxy} - density of ortho xylene, ξ - electronegativity

Fig. 3 reports, DTA spectra of the $Ba_{(10-x)}Ni_xLa_{30}Si_{60}$ glasses. The glass transition (T_g), and crystallization (T_c) temperature positions are identified from the spectra. And thermal stabilities of glasses are computed with the help of glass transition (T_g), and crystallization (T_c) temperature. Thermal stabilities of glasses projected in the inset of the figure number 03. Observed results reveal a glass with 0.6 mol% NiO concentration exhibiting the highest in thermal stability grades. All the exothermic and endothermic thermograms variations are due to enthalpy change in the $Ba_{(10-x)}Ni_xLa_{30}Si_{60}$ glasses [13,14]. All the reports include both physical and thermal stability values of glasses projected in Table.1. Structural characterization, which includes diffraction, morphology, chemical, and thermal analysis, suggests samples' glassy behavior.

Fig. 4 reports FT-IR spectra of $Ba_{(10-x)}Ni_xLa_{30}Si_{60}$ glasses. Observed spectra exhibited well resolved following bands due to silicate, lanthanum, and nickel units at different wavenumber regions [15-18].

(a). Si–O–Si Asymmetrical (~ 1025 to 1043 cm^{-1}) stretching

(b). Si–O–Si Symmetrical (~ 843 to 858 cm^{-1}) stretching

(c). Si–O–Si Rocking /bending (~ 474 to 462 cm^{-1}) vibrations

(d). La–O–La (~ 640–645 cm^{-1}) linkages

(e). Ni–O–Ni Specific (~ 534 to 539 cm^{-1}) stretching vibrations

The glass with a 0.6 % of NiO concentration found to be highest in the $Ba_{(10-x)}Ni_xLa_{30}Si_{60}$ glasses exhibiting the highest shift in wavenumber positions of all the silicate, lanthanum, barium and nickel structural units.

The Fig. 5(a), and Fig. 5(b) illustrates, the elastic properties of $Ba_{(10-x)}Ni_xLa_{30}Si_{60}$ glasses. The following mathematical equations are used to calculate all the parameters [19, 21]. The glass with 0.6 mol% NiO concentration observed to be best in the values of mechanical properties of glasses.

Elastic coefficient (A) = $D (S_1)^2$,

Shear modulus (W) = $D (S_2)^2$,

Bulk modulus (X) = A – (4/3W),

Young's modulus (B) = $(1 + \sigma)$ 2W,

Poisson's ratio (Z) = (A– 2W) / 2(A – W)

Micro hardness (Ω) = B (1 – 2Z) / 6(1 + Z)

Where, S_1 – longitudinal velocity, and S_2 – shear velocity. The evaluated all the information with regard to mechanical properties of the $Ba_{(10-x)}Ni_xLa_{30}Si_{60}$ glasses presented in table number 02.

Fig. 6(a) reports the optical absorption of current glasses. And the OBE of glasses found at ~ 307.5 nm. Glass 'ξ_6' observed to be highest among all the values of the present series of materials. Analysis reveal NiO absorption bands such as $^3A_2$ (F) → $^3T_1$(P), $^3T_1$ (F) → $^3T_1$(P), $^3A_2$ (F) → $^1T_2$(D) & $^3T_1$ (F) → $^3A_2$(F) around at 470, 685, 740 and 1045 nm wavelength range [22]. Fig. 6(b) reports Tauc plots of glasses, which will help to find band gap's values of glasses. In this view, the glass with 0.6 mol% NiO concentration observed to be highest among all other glasses. Urbach energy evaluations are also reported and analysed for a better description of glasses [23]. Absorption spectra evaluations, identifications, and results of current $Ba_{(10-x)}Ni_xLa_{30}Si_{60}$ glasses reported in table number 03.

Fig. 7(a) reports photoluminescence of glasses. Luminescence parameters such as cross-section, transition probability analogous to the emissive bands $^3T_1$(P) → $^3A_2$(F) and $^3T_1$(P) → $^3T_2$(F) around at 565 and 695 nm wavelength range [24] are evaluated and analysed. The glass with 0.6 mol% NiO concentration observed to be highest among all the values of various luminescent quantities of glasses. The subsequent equations [22] are used to determine luminescence results

$A = [8\nu^2 \times 10^6] / (e)^2$;

$\delta = [(\lambda)^4 A] / [8\pi \Delta\lambda\, c\, (\mu)^2]$;

Where, λ-wavelength; $\Delta\lambda$ - peak half width; A- transition probability; μ-refractive index; δ - cross section; ν - frequency; c - velocity of light; e - electron charge;

Fig. 7(b) indicates the colour Chromacity report of glass with 0.6 mol% NiO concentration. Chromacity analysis relative to transitions $^3T_1$(P) → $^3A_2$(F) and $^3T_1$(P) → $^3T_2$(F) suggests orange emission. However, it is changing with NiO concentration. In this view, the glass code 'ξ_6' observe to exhibit the highest shift towards the red region among all the values of the present series of materials. Improved efficiency up to 0.6 mol % of NiO intensity is due to an enlarged number of octahedral Ni^{2+} ions within the glasses [25]. Fig. 8 illustrates D.C. Conductivity variations with the inverse of increasing temperature. Observed results are almost

linear. Insect (a), and (b) of the figure signifies the variation in D.C. Conductivity and A.E. with NiO increasing concentration. Observed DC Conductivity increased up to 0.6 mol% of NiO increasing concentration. Whereas analysed, A.E. found to be decreasing until 0.6 mol% of NiO increasing concentration [26]. All the evaluations concerning D.C. Conductivity measurements are found to be best for the glass with 0.6 mol% of NiO concentration. The detailed information concerning D.C. Conductivity measurements of the $Ba_{(10-x)}Ni_xLa_{30}Si_{60}$ glasses are furnished in table number 05.

Fig. 9 reports thermoluminescence spectra of the $Ba_{(10-x)}Ni_xLa_{30}Si_{60}$ glasses, recorded within the temperature range of 27 to 380 ^oC and under 30 kGy of gamma irradiation. Observed results reveal a maximum thermoluminescence effect in the glass test arranged with x = 0.6 mol% (ξ_6). T.L. glow curves revealing extreme intensity at ~ 240 ^oC. The subsequent equations [27-29] are used to analysed the trap-depth parameters

$E_\theta = C_\theta \left(\frac{KT_m^2}{\tau}\right) 2KT - b_\theta(2KT_m)$; Where, $\theta = \tau, \delta, \text{and } \omega$

$S = \frac{\beta E}{KT_m^2} \exp\left(\frac{E}{kT_m}\right)[1 + (b-1)\Delta_m]^{-1}$;

where,

$\Delta_m = \frac{2k\,T_m}{E}$; $\tau = T_m - T_1$, $\delta = T_2 - T_m$, and $\omega = T_2 - T_1$;

T_m – peak temperature maximum; T_1 - left side temperature intercept on glow curve at $T_m/\sqrt{2}$ value;

T_2 - right side temperature intercept on glow curve at $T_m/\sqrt{2}$ value;

μ_s – symmetry;

$\beta -$ heating rate;

C_t, C_δ , and C_w are [1.51 + 3(m-0.42)], [0.97 + 7.3 (m-0.42)], & [2.52 + 10.2 (m-0.42)];

b_t, b_δ , and b_w are [1.51 + 3(m-0.42)], 0 and 0;

With the increase of NiO weight% from 0 to 1 mol %, the TL measurements of the $Ba_{(10-x)}Ni_xLa_{30}Si_{60}$ glasses found to be increased, and the glass with 0.6 % of NiO content found to be best in the results. The detailed information of the TL reports of glasses are furnished in table number 06.

IV. DISCUSSION

Essentially, SiO_2 is a regular class of glass former, widely available in amorphous form and pure class form silica observed in nature as quartz. The tetrahedrons in SiO_2 geometry are observed to be interconnected with mutual corners sharing. Usually, SiO_2 in its amorphous form will be preferred for glass production [30,31]. Generally, amorphous silica (or) precipitated the acidification of sodium silicate solutions obtains silica.

$$Na_2Si_3O_7 + H_2SO_4 \rightarrow 3SiO_2 + Na_2SO_4 + H_2O$$

Usage of La_2O_3 in SiO_2 glasses improves the hardness, refractive index, and density of optical glasses. It is also used to improve thermo and piezoelectric characteristics of SiO_2 glass. SiO_2 glass phosphors, conductive ceramics, and dielectrics inclusive of La_2O_3 are valuable photoelectronic resources. Naturally, La_2O_3 has M_2O_3 hexagonal symmetry at low temperatures. At this state, La^{3+} ions

are involved with seven octahedral located O^{2-} ions. La_2O_3 production involves two steps – hydrolysis followed by dehydration [32].

$$02\ (LaCl_3) + 03\ (H_2O) \rightarrow La(OH)_3 + 03\ HCl$$

$$02\ La(OH)_3 \rightarrow La_2O_3 + 03\ (H_2O)$$

Inclusive of BaO involves very actively with Ba^{2+} ions, which improves Ba-O-Ba linkages by breaking Si-O-Si and La-O-Si linkages, which further lead to improvement of non-bridging oxygens within the glass network [33]. Fig.10 reports structural changes in barium lanthanum silicate glass with the addition of NiO. The addition of NiO actively involves with Ni^{2+} ions within silicate glass network produce Ni-O-Si linkages, which further influence all other Si^{4+}, La^{3+}, and Ba^{2+} ions within the glass network and improves non-bridging oxygen's [34]. X-ray diffraction reports reveal the amorphous nature of existing glasses. And supportively, surface morphology and differential thermal analysis study back too. Chemical analysis studies reveal the significance and existence of all the chemicals with suitable weight %, which have been chosen for present synthesis. FT-IR analysis supports all the existence various chemicals such as Si–O–Si Asymmetrical (~ 1025 to 1043 cm^{-1}), Si–O–Si Symmetrical (~ 843 to 858 cm-1), Si–O–Si bending (~ 474 to 462 cm^{-1}), La–O (~ 645 cm^{-1}) distorted octahedral and Ni–O–Ni Specific (~ 534 to 539 cm^{-1}) stretching vibrational units. Glass with a 0.6 % of NiO concentration found to be highest in the $Ba_{(10-x)}Ni_xLa_{30}Si_{60}$ glasses exhibiting the highest shift in wavenumber positions of all the silicate, lanthanum, barium and nickel structural units due to steady inter-ionic forces between Ni^{2+} ions to Si^{4+}, La^{3+}, and Ba^{2+} ions. Uncertainties in the magnitudes of the interstitial holes and dissimilarity in the coordination of Ni^{2+} ions to Si^{4+}, La^{3+}, and Ba^{2+} ions is the reason for the variation of density, molar volume, field strength, refractive index, and polarizability of ξ - series of glasses. Steady inter-ionic forces between Ni^{2+}ions to Si^{4+}, La^{3+}, and Ba^{2+} ions lead to the thermal stability of existing materials. This is found to be highest for a glass with a 0.6 % of NiO concentration. Change in enthalpy within the glass network results from the difference in DTA thermogram peak intensities [35]. Naturally, the glasses are extreme elastic behavior under any attentive glass formation. And the numerous elastic modulus of glass materials is an interdependent allocation of intermolecular control. In some glass (or) glass-ceramic materials, the elastic module improves through a predictable degree of molecular density. Replacement of Ba^{2+} ions by divalent Ni^{2+} ions within materials causes higher orders of variations in elastic modulus (bulk, shear, and young's). Further, which leads to a high degree of covalent bonding within a glass of 0.6 % of NiO concentration, increased atomic density, and variations in interstitial defects could be another reason for increasing the bulk, shear, and young's module. The Microhardness of present glasses prescribes additional information about covalently interlinked structure [36].

Observed absorption results of band gaps of the present ξ - series of glasses found to be least for the glass code concentrated with 0.6 % of nickel oxide. Ba^{2+} and Ni^{2+} ions improve bonding defects and the number of non-bridging oxygen's, which may induce depolymerization within the glass host. Ni^{2+} ions form donor ions, which are overlapped with excited states of electrons which are primarily trapped by Ni^{2+} ionic sites. This may further lead to impurity energy band enters into the actual optical bandgap. Absorption edge shifts towards a longer wavelength side due to a decrease in values of the optical bandgap. Suppose the NiO concentration exceeds 0.6 mol%, the width of impurity band decreases, which leads to optical absorption edge shifts into higher

wavelength side, which results from the increase in values of the optical bandgap. Well resolved bands such as $^3A_2(F) \rightarrow {}^3T_1(P)$ and $^3A_2(F) \rightarrow {}^1T_2(D)$ reveal octahedral, whereas the other spectral bands $^3T_1(F) \rightarrow {}^3T_1(P)$ and $^3T_1(F) \rightarrow {}^3A_2(F)$ are tetrahedral. Optical absorption spectra reveal Ni^{2+} ions in both octahedral and tetrahedral sites with the present ξ_6 - series of materials. The intensity increase in absorption bands suggests the Ni^{2+} ions prevailingly occupy octahedral positions, whereas the other bands relatively less intense suggest tetrahedral sites. All the observations suggest improvement of ionic environment lead to covalent nature of present glassy materials and it highest for glass code with 0.6 mol% of NiO concentration [37,38]. In the present ξ - series of materials, Ni^{2+} ions prefer to dominate tetrahedral positions with NiO_4 structural units in the glass network along with octahedral positions indicating that the number of octahedral sites is relatively less than the number of tetrahedral sites. In current glass materials, the bandgap values are decreasing up to 0.6 mol% NiO concentration. Unsteady interionic forces between La^{3+} ions to Ni^{2+} ions lead to depolymerization within the glassy network. Which further induces additional orders of bonding defects and NBO's. Enlargement of ionized donors influence overlapped conduction states which include electrons primarily trapped with Ni^{2+} ions with 3d orbitals lead to a decrease in optical bandgap [39,40]. The absorption edge of glasses shifting with the increase of NiO concentration is due to uncertain interionic forces between La^{3+} and Ni^{2+} ions within the glass host. However, the decrease in width of the impurity band beyond the 0.6 mol% of NiO leads to an increase in the bandgap value. Octahedral positional Ni^{2+} ions are responsible for enhanced luminescence in the present ξ - series of materials. Glass with 0.6 mol% of NiO concentration showing highest luminescence output having highest octahedral tendency. Intensities of luminescence bands such as $^3T_1(P) \rightarrow {}^3A_2(F)$ and $^3T_1(P) \rightarrow {}^3T_2(F)$ show redshift with an increase in NiO concentration up to 0.6 mol% due to octahedral tendency. Above 0.6 mol% of NiO concentration, there is a blue shift due to Ni^{2+} ions. Redshift up to 0.6 mol% of NiO in the present ξ- series of materials is due to the decrease in the strength of crystal field stabilization energy around Ni^{2+} octahedral ions, which further decreases the separation between ground to excited states. Blueshift beyond the 0.6 mol% of NiO concentration in the present ξ - series of materials is due to the increasing strength of crystal field stabilization energy around Ni^{2+} octahedral ions, which further increases the separation between ground to excited states [41,42]. All the values of transition probability and cross-section about the emission of the present series of materials show the highest value for glass with 0.6 mol% of NiO concentration due to the highest interionic balance and resultant force between Ni^{2+} ions to Ba^{2+} La^{3+} and Si^{4+} ions. Linear relation between D.C. Conductivity with increased inverse temperature in the present ξ - series of materials suggesting that the linear thermally exciting movement of the charge carriers for conduction [43, 44]. An increase in the values of D.C. Conductivity and decrease in the values of A.E. up to 0.6 mol% of NiO concentration suggest a higher rate of polaron hopping and ionic transport phenomenon within the present ξ- series of materials. Mixed ionic and electronic conduction effects cause an increase in the value of D.C. Conductivity and a decrease in the values of A.E. up to 0.6 mol% of NiO concentration. In comparison, decreasing D.C. Conductivity and decrease in the values of A.E. after 0.6 mol% of NiO concentration. Both analyses suggest dissimilar conduction phenomena on the two sides of the present chemical composition. Such variations in the values of both D.C. Conductivity and A.E. of the present ξ - series of materials due to conformed mobility of both Ba+ and Ni^{2+} ions [45,46]. Generally, lanthanum trioxide exhibits (La/Si)-O tri-clusters. Ba^{2+} ions and octahedral (La/Si)-O6 tri-clusters dislocate silicate linkages and induce binding defects. The addition of La_2O_3 improves the structural defects within the glass network. Once present

materials are subjected to thermal energy, the electrons are liberated from La^{3+}, Si^{4+}, Ni^{2+}, and Ba^{2+} ions. Later, recombined of these electrons with holes cause thermoluminescence. Glass 'ξ_6' was observed to be highest among all the trap depth findings of materials. Predominantly, interstitial positions of both the valence states corresponding to the Ni^{2+} ions cause a higher imperative nephelauxetic effect within the 3d levels of nickel ions contributes to enhanced T.L. emission [47,48]. Octahedral LaO_6 and NiO_6 units act as modifiers and induce binding defects. And increase of La–O–Si, Ba–O–Si and Ni–O–Si linkages could lead substitute TL emission. All the analyses concerning the increased no of octahedral LaO_6 and NiO_6 units induce interstitial and volume defects, which cause higher disorders within the glassy network. T.L. output intensities are dependent on La^{3+}, Si^{4+}, Ni^{2+}, and Ba^{2+} ions site symmetry, order of La-O and Ni-O bond linkages, and balanced interatomic forces within the glass network. Thermoluminescence dosimetry is the widely used means of dosimetric measurements, especially for personnel monitoring of radiation workers. The materials used for personnel monitoring should meet several requirements like high sensitivity, low fading, linear response over a wide range of doses, and no energy dependence. A single material may not satisfy all the requirements for personnel dosimetry. The field evolves by developing new materials or improving the characteristics of existing phosphors by using different synthesis techniques or changing the dopants. Most inorganic compounds exhibit thermoluminescence. However, to use a phosphor for dosimetric applications, it should qualify some properties, limiting the choice to only a handful of materials. Some of the most desirable properties that qualify a phosphor for dosimetric applications are a high concentration of electrons and hole traps and high efficiency in the recombination process resulting in intense light emission upon heating (high sensitivity). The variation in the glow curves of glasses are studied with increased NiO%, and the optimum concentration was determined for each of the glasses. Also, the other dosimetric parameters like reusability, storage stability, light sensitivity, reproducibility in synthesis, etc., are studied. Lithium tetraborate is one of the TL phosphors studied for a long time since its first introduction due to its tissue equivalence. But the $Ba_{(100-x)}Ni_xLa_{30}Si_{60}$ glasses synthesized by using the melt quenching technique have a high-temperature glow peak and hence benefit minor fading. Hence a detailed investigation has been carried out on this material concerning increasing the TL intensity and dose-response. The increase of NiO weight% from 0 to 1 mol % improves the structural defect centers within the glasses. Once glasses are subjected to the thermal energy, the electrons are liberated from La^{3+}, Si^{4+}, Ni^{2+} and Ba^{2+} ions. Later, recombined these electron centers with hole trap centers cause thermoluminescence. Glass with 0.6 mol% of NiO concentration was observed to be highest among all the trap depth findings of glasses. Predominantly, interstitial positions of both the valence states corresponding to the Ni^{2+} ions cause a higher imperative nephelauxetic effect within the 3d levels of Ni^{2+} ions, contribute to enhanced TL emission. The Octahedral NiO_6 units act as modifiers and induce binding defects. And the increase of La–O–Si, Ba–O–Si, and Ni–O–Si linkages could enhance TL emission. The increased no of octahedral NiO_6 units induces interstitial and volume defects, which cause higher order of disorder within the glasses. TL output intensities are dependent on La^{3+}, Si^{4+}, Ni^{2+} and Ba^{2+} ions site symmetry, order of Ba-O, La-O, and Ni-O bond linkages, and balanced interatomic force within the glasses.

V. CONCLUSION

In the present work, we have synthesized multifunctional $Ba_{(10-x)}Ni_xLa_{30}Si_{60}$ glasses. Various structural, elastic, photo-electronic, and thermoluminescent techniques are used to characterize the glasses. Under DTA Studies, evaluated thermal stabilities of glasses

found to be highest for a glass with 0.6 mol% NiO concentration, which suggests higher order of intermolecular force and covalence in between Ni^{2+} ions to all other Ba^{2+}, La^{3+} and Si^{4+} ions in a glass with 0.6 mol% NiO concentration. Ultrasonic velocities were recorded to evaluate the elastic characteristics of glasses. Under elastic characterization, the evaluated microhardness (~ 2.62 GPa) range suggests higher rigidity and elastic strength of glasses. Refractive index (~1.649), Optical bandgap (~ 1.98 eV), transition probability (~1.42 S^{-1}) and cross-section (~ 0.901 x 10^{-34} cm^2) values analogous to the transition $^3T_1(P) \rightarrow {}^3A_2(F)$ of glass with 0.6 mol% NiO concentration is a highly suggestable glass for photonic use. D.C. conductivity and thermoluminescence studies of glasses reported; Observed, dc conductivity (~ 4.23 x 10^{-8} ohm^{-1} cm^{-1}), and A.E. (~ 2.206 eV) evaluations of glass with 0.6 mol% NiO concentration is a beneficial glass in electronics. Trap depth parameters, shape symmetry (~ 0.514) factor and low AE's (E_τ = 1.833, E_δ = 1.794 & E_ω = 1.822) of a glass with 0.6 mol% NiO concentration under thermoluminescence studies is a useful TL asset. Based on structural, mechanical, thermoluminescent, and opto-electronic studies of glasses recommend that glass with 0.6 mol% NiO concentration is a desirable resource for thermoluminescent, and opto-electronic use.

Acknowledgments

The authors thank Shri. K. Abhijith Rao, CEO : SNIST-JNT University for providing some financial assistance by means of internal R and D Project grants.

Reference

[1] C. Martinet, M. Heili, V. Martinez, G. Kermouche, G. Molnar, N. Shcheblanov, E. Barthel, A. Tanguy, Highlighting the impact of shear strain on the SiO_2 glass structure: From experiments to atomistic simulations, Journal of Non-Crystalline Solids, 533 (2020) 119898, https://doi.org/10.1016/j.jnoncrysol.2020.119898.

[2] M. Ficheux, E. Burov, G. Aquilanti, N. Trcera, V. Montouillout, L. Cormier, Structural evolution of high zirconia aluminosilicate glasses, Journal of Non-Crystalline Solids, 539 (2020) 120050 https://doi.org/10.1016/j.jnoncrysol.2020.120050.

[3] Shahriar Iftekhar, Jekabs Grins, Mattias Edén, Composition–property relationships of the La_2O_3–Al_2O_3–SiO_2 glass system, Journal of Non-Crystalline Solids, 356, 20, 2010, 1043-1048, https://doi.org/10.1016/j.jnoncrysol.2010.01.017.

[4] Jiansheng Xie, Minghui Zhang, Rongting Guo, Ying Shi, Xuechao Liu, Xiuhong Pan, Kun Chen, Weijie Deng,Investigation of optical and thermal properties in Er^{3+}-doped Ga_2O_3-La_2O_3-Ta_2O_5 glasses fabricated by container less solidification, Journal of Alloys and Compounds, 872 (2021) 159651 https://doi.org/10.1016/j.jallcom.2021.159651.

[5] Liliya Vladislavova, Christian Thieme, Tilman Zscheckel, Thomas Höche, Christian Rüssel, Crystallization of $Ba_{1-x}Sr_xZn_2Si_2O_7$ from the BaO/SrO/ZnO/SiO_2 glass system: Effect of platinum and Sb_2O_3 on nucleation, Journal of Alloys and Compounds, 793 (2019) 705-714, https://doi.org/10.1016/j.jallcom.2019.04.034.

[6] En-Lai Zhao, Shi-Xi Zhao, Xia Wu, Jing-Wei Li, Lü-Qiang Yu, Ce-Wen Nan, Guozhong Cao, Electrochemical performance of Li_2O-V_2O_5-SiO_2-B_2O_3 glass as cathode material for lithium ion batteries, Journal of Materiomics, 5 4 (2019) 663-669 https://doi.org/10.1016/j.jmat.2019.05.002.

[7] Sea-Fue Wang, Yung-Fu Hsu, Yueh-Chi Hsieh, Effects of La_2O_3, Nd_2O_3, NiO and CoO additions on the characteristics of SiO_2–Al_2O_3–Y_2O_3–ZnO glass seals for intermediate temperature solid oxide fuel cells, International Journal of Hydrogen Energy, 40, 8, 2015, 3338-3347, https://doi.org/10.1016/j.ijhydene.2015.01.045.

[8] B. Suresh, M. Srinivasa Reddy, A. Siva Sesha Reddy, Y. Gandhi, V. Ravi Kumar, N. Veeraiah, Spectroscopic features of Ni^{2+} ion in PbO–Bi_2O_3–SiO_2 glass system, Spectrochimica Acta Part A: Molecular and Biomolecular Spectroscopy, 141, 2015 263-271 https://doi.org/10.1016/j.saa.2015.01.058.

[9] Christian Thieme, Christian Rüssel, High thermal expansion of crystallized glasses in the system BaO–ZnO–NiO–SiO2, Ceramics International, 41, 10, Part A, (2015) 13310-13319 https://doi.org/10.1016/j.ceramint.2015.07.114.

[10] Sea-Fue Wang, Yung-Fu Hsu, Yueh-Chi Hsieh, Effects of La_2O_3, Nd_2O_3, NiO and CoO additions on the characteristics of SiO_2–Al_2O_3–Y_2O_3–ZnO glass seals for intermediate temperature solid oxide fuel cells, International Journal of Hydrogen Energy, 40, 8, 2015, 3338-3347 https://doi.org/10.1016/j.ijhydene.2015.01.045.

[11] Padala Ashok, et.al., $[Sb_2O_3]_x$ $[Al_2O_3]_{y-x}$ composite influence on Ho_2O_3 doped PbO - SiO_2 glasses for optical use, Optik, 206, (2020) 164367 https://doi.org/10.1016/j.ijleo.2020.164367.

[12] Y. Al-Hadeethi, M.I. Sayyed, J. Kaewkhao, Bahaaudin M. Raffah, Rahma Almalki, R. Rajaramakrishna, Mahmoud A. Hussein, Physical, optical properties and radiation shielding studies of xLa_2O_3-(100-x)B_2O_3 glass system, Ceramics International, 46 4 (2020) 5380-5386 https://doi.org/10.1016/j.ceramint.2019.10.293.

[13] J.L. Amorós, E. Blasco, A. Moreno, N. Marín, C. Feliu, Sinter-crystallisation kinetics of a SiO_2–Al_2O_3–CaO–MgO–SrO glass-ceramic glaze, Journal of Non-Crystalline Solids, 532 (2020) 119900 https://doi.org/10.1016/j.jnoncrysol.2020.119900.

[14] Ho Kim Dan, Nguyen Minh Ty, Tran Duy Tap, Ha Xuan Vinh, L.T. Vinh, Qing Jiao, Dacheng Zhou, Jianbei Qiu, Effects of Al^{3+}/La^{3+} ratio on the DSC/DTA and luminescence properties of Bi-doped lanthanum aluminosilicate glasses, Infrared Physics & Technology, 103 (2019) 103072 https://doi.org/10.1016/j.infrared.2019.103072.

[15] Yuya Isokawa, Daisuke Nakauchi, Go Okada, Noriaki Kawaguchi, Takayuki Yanagida, Radiation induced luminescence properties of Ce-doped Y_2O_3-Al_2O_3-SiO_2 glass prepared using floating zone furnace, Journal of Alloys and Compounds, 782 (2019) 859-864 https://doi.org/10.1016/j.jallcom.2018.12.245.

[16] Bikram Konar, Dong-Geun Kim, In-Ho Jung, Critical thermodynamic optimization of the Li_2O-Al_2O_3-SiO_2 system and its application for the thermodynamic analysis of the glass-ceramics, Journal of the European Ceramic Society, 38 11 (2018) 3881-3904 https://doi.org/10.1016/j.jeurceramsoc.2018.04.031.

[17] G Ravi, M Sarasija, D Ayodhya, et al. Facile synthesis, characterization and enhanced catalytic reduction of 4-nitrophenol using NaBH4 by undoped and Sm^{3+}, Gd^{3+}, Hf^{3+} doped La2O3 nanoparticles. Nano convergence 6, 12 (2019) https://doi.org./10.1186/s40580-019-018-6

[18] Venkata Sekhar, L. Pavić, A. Moguš-Milanković, Valluri Ravi Kumar, A. Siva Sesha Reddy, G. Naga Raju, N. Veeraiah, Dielectric dispersion and impedance spectroscopy of NiO doped Li_2SO_4–MgO–P_2O_5 glass system, Journal of Alloys and Compounds, 824 (2020) 153907 https://doi.org/10.1016/j.jallcom.2020.153907.

[19] Shams A.M. Issa, Atif Mossad Ali, G. Susoy, H.O. Tekin, Yasser B. Saddeek, Reda Elsaman, H.H. Somaily, H. Algarni, Mechanical, physical and gamma ray shielding properties of xPbO-(50-x) MoO_3–$50V_2O_5$ ($25 \leq x \leq 45$ mol %) glass system, Ceramics International, 46 12 (2020) 20251-20263 https://doi.org/10.1016/j.ceramint.2020.05.107.

[20] Q.Y. Zhang, W.J. Zhang, W.C. Wang, Z.H. Jiang, Calculation of physical properties of glass via the phase diagram approach, Journal of Non-Crystalline Solids, 457 (2017) 36-43 https://doi.org/10.1016/j.jnoncrysol.2016.11.005.

[21] Ravi Kumar Guntu, Nd_2O_3 Influenced Al_2O_3 & Sb_2O_3 Functional PbO-SiO2 Glass Materials, 1.06 μm Photonic Resource, Materials Science and Engineering: B, 262, 2020, 114784, https://doi.org/10.1016/j.mseb.2020.114784.

[22] Y. Al-Hadeethi, M.I. Sayyed, J. Kaewkhao, Bahaaudin M. Raffah, Rahma Almalki, R. Rajaramakrishna, Mahmoud A. Hussein, Physical, optical properties and radiation shielding studies of xLa_2O_3-(100-x)B_2O_3 glass system, Ceramics International, 46 4 (2020) 5380-5386 https://doi.org/10.1016/j.ceramint.2019.10.293.

[23] Y. Gandhi, N. Krishna Mohan, N. Veeraiah, Role of nickel ion coordination on spectroscopic and dielectric properties of ZnF_2–As_2O_3–TeO_2:NiO glass system, Journal of Non-Crystalline Solids, 357 3 (2011) 1193-1202 https://doi.org/10.1016/j.jnoncrysol.2010.11.016.

[24] Ravi Kumar Guntu, Luminescence and dielectric properties of Ni^{2+} ions added to calcio yttria borophosphate glasses for optoelectronic uses, Journal of Luminescence, 209, 2019, 258-266, https://doi.org/10.1016/j.jlumin.2019.01.051.

[25] G. Ravi Kumar, M. Koteswara Rao, T. Srikumar, M.C. Rao, V. Ravi Kumar, N. Veeraiah, Ch.Srinivasa Rao, Spectroscopic, dielectric dispersion and dc conductivity studies of Sb_2O_3 doped lithium fluoro borophosphate glasses mixed with small concentrations of NiO, Journal of Alloys and Compounds, 752 2018, 179-190, https://doi.org/10.1016/j.jallcom.2018.04.165.

[26] Padmanabham, Y. Gandhi, T. Satyanarayana, N. Veeraiah, Spectroscopic and dielectric properties of crystallized PbO–Sb_2O_3–As_2O_3:NiO glass system, Journal of Alloys and Compounds, 488 1 (2009) 400-408 https://doi.org/10.1016/j.jallcom.2009.08.148.

[27] Ravi Kumar Guntu, V. Venkatramu, Ch. Srinivasa Rao, V. Ravi Kumar, Structure, and opto-dielectric investigations of Cu^{2+}-doped calcium bismuth silicate glass ceramics, Optical Materials, 113, 2021, 110876, https://doi.org/10.1016/j.optmat.2021.110876.

[28] Ho Kim Dan, Nguyen Minh Ty, Tran Duy Tap, Ha Xuan Vinh, L.T. Vinh, Qing Jiao, Dacheng Zhou, Jianbei Qiu, Effects of Al^{3+}/La^{3+} ratio on the DSC/DTA and luminescence properties of Bi-doped lanthanum aluminosilicate glasses, Infrared Physics & Technology, 103 (2019) 103072 https://doi.org/10.1016/j.infrared.2019.103072.

[29] Padala Ashok, et.al 'Influence of Al^{3+} and Sb^{3+} ions on thermo and photoluminescence properties of Pr_2O_3 doped PbO – SiO_2 glasses for optical use' Journal of Luminescence, 227 (2020) 117473 https://doi.org/10.1016/j.jlumin.2020.117473.

[30] P.A. Loiko, O.S. Dymshits, A.A. Zhilin, I.P. Alekseeva, K.V. Yumashev, Influence of NiO on phase transformations and optical properties of ZnO–Al_2O_3–SiO_2 glass–ceramics nucleated by TiO_2 and ZrO_2. Part II. Optical absorption and luminescence, Journal of Non-Crystalline Solids, 376 (2013) 99-105, https://doi.org/10.1016/j.jnoncrysol.2013.05.031.

[31] I. Alekseeva, O. Dymshits, M. Tsenter, A. Zhilin, Influence of various alkali and divalent metal oxides on phase transformations in NiO-doped glasses of the Li_2O–Al_2O_3–SiO_2–TiO_2 system, Journal of Non-Crystalline Solids, 357 (2011) 2209-2214, https://doi.org/10.1016/j.jnoncrysol.2010.12.065.

[32] T. Srikumar, M.G. Brik, Ch. Srinivasa Rao, N. Venkatramaiah, Y. Gandhi, N. Veeraiah, Emission features of Ho^{3+} ion in Nb_2O_5, Ta_2O_5 and La_2O_3 mixed Li_2O–ZrO_2–SiO_2 glasses, Physica B: Condensed Matter, 406, 19, 2011, 3592-3598, https://doi.org/10.1016/j.physb.2011.06.046.

[33] Haiyang Zhu, Renli Fu, Simeon Agathopoulos, Jun Fang, Guojun Li, Qinjiang He, Crystallization behaviour and properties of BaO-CaO-B_2O_3-SiO_2 glasses and glass-ceramics for LTCC applications, Ceramics International, 44, 9, 2018, 10147-10153, https://doi.org/10.1016/j.ceramint.2018.03.003.

[34] V. Prasad, B. Suresh, M. Kostrzewa, Y. Gandhi, A. Ingram, A. Siva Sesha Reddy, V. Ravi Kumar, N. Veeraiah, Dielectric dispersion, dipolar relaxation and a.c. conduction phenomena of NiO doped lead bismuth silicate glass system, Journal of Non-Crystalline Solids, 500 (2018) 460-467 https://doi.org/10.1016/j.jnoncrysol.2018.09.002.

[35] Pratthana Intawin, Surapong Panyata, Arnon Kraipok, Tawee Tunkasiri, Sukum Eitssayeam, Kamonpan Pengpat, Effects of TiO_2 content and thermal parameters on crystallization kinetics and mechanical properties of phosphate based glass system, Thermochimica Acta, (2020) 178699 https://doi.org/10.1016/j.tca.2020.178699.

[36] Jianlei Liu, Lei Han, Zhiwei Luo, Qianxing Huang, Xi He, Changwei Lin, Taoyong Liu, Cui Li, Anxian Lu, Non-alkali glass substrate with improved mechanical properties for display devices, Journal of Non-Crystalline Solids, 524 (2019) 119610 https://doi.org/10.1016/j.jnoncrysol.2019.119610.

[37] Zahra Jamili-Shirvan, Mohsen Haddad-Sabzevar, Jalil Vahdati-Khaki, Ke-Fu Yao, Mechanical and thermal properties of identified zones at a Ti-based bulk metallic glass weld spot jointed by friction stir spot welding (FSSW), Journal of Non-Crystalline Solids 544 (2020) 120188 https://doi.org/10.1016/j.jnoncrysol.2020.120188.

[38] Jingbo Yu, Yi Gu, Qian Zhang, Zhiwei Luo, Anxian Lu, A new type of NiO-doped phosphate glass with excellent Faraday effects, Materials Letters, 212 (2018) 25-27 https://doi.org/10.1016/j.matlet.2017.10.056.

[39] O.A. Zamyatin, M.F. Churbanov, J.A. Medvedeva, S.A. Gavrin, E.V. Zamyatina, A.D. Plekhovich, Glass-forming region and optical properties of the TeO_2 – ZnO – NiO system, Journal of Non-Crystalline https://doi.org/10.1016/j.jnoncrysol.2017.10.005.

[40] M.S. Al-Buriahi, A.S. Abouhaswa, H.O. Tekin, C. Sriwunkum, F.I. El-Agawany, T. Nutaro, Esra Kavaz, Y.S. Rammah, Structure, optical, gamma-ray and neutron shielding properties of NiO doped B_2O_3–$BaCO_3$–Li_2O_3 glass systems, Ceramics International, 46 2 (2020) 1711-1721 https://doi.org/10.1016/j.ceramint.2019.09.144.

[41] W.C. Wang, R. Zhou, H.Q. Le, Q.Y. Zhang, L. Wondraczek, Ni-doped fluorosulfates with broad NIR luminescence, Journal of Luminescence, 210 (2019) 457-463 https://doi.org/10.1016/j.jlumin.2019.03.007.

[42] Zhuo-hao Xiao, Xin-yuan Sun, Kun Liu, Wen-yan Luo, Yun-zhi Wang, Min-hua Luo, Run-lin Han, Yan Liu, Crystallization behaviors, thermo-physical properties and seal application of Li2O–ZnO–MgO–SiO_2 glass-ceramics, Journal of Alloys and Compounds, 657 (2016) 231-236. https://doi.org/10.1016/j.jallcom.2015.10.106.

[43] Vinh V. Le, Giang T. Nguyen, Molecular dynamics simulation of structural transformation in SiO_2 glass under densification, Journal of Non-Crystalline Solids, 505 (2019) 225-233 https://doi.org/10.1016/j.jnoncrysol.2018.11.016.

[44] Manuela Alejandra Zalapa-Garibay, David Torres-Torres, Ana María Arizmendi-Morquecho, Simón Yobanny Reyes-López, Effect of NiO and MoO_3 addition on the crystallinity and mechanical properties of α-cordierite and β-cordierite in the MgO-Al_2O_3-SiO_2 system, Results in Physics, 13 (2019) 102227, https://doi.org/10.1016/j.rinp.2019.102227.

[45] Sanjib Bhattacharya, Ranadip Kundu, Anindya Sundar Das, Debasish Roy, Interpretation of dc and ac conductivity of Ag_2O–SeO_2–MoO_3 glass-nanocomposite-semiconductor, Materials Science and Engineering: B, 197 (2015) 51-57 https://doi.org/10.1016/j.mseb.2015.02.009.

[46] M.Y. Hassaan, M.G. Moustafa, K. Osouda, S. Kubuki, T. Nishida, ^{57}Fe and ^{119}Sn Mössbauer, XRD, FTIR and DC conductivity study of $Li_2OFe_2O_3SnO_2P_2O_5$ glass and glass ceramics, Journal of Alloys and Compounds, 765 (2018) 121-127 https://doi.org/10.1016/j.jallcom.2018.06.207.

[47] Sea-Fue Wang, Yung-Fu Hsu, Yueh-Chi Hsieh, Effects of La_2O_3, Nd_2O_3, NiO and CoO additions on the characteristics of SiO_2–Al_2O_3–Y_2O_3–ZnO glass seals for intermediate temperature solid oxide fuel cells, International Journal of Hydrogen Energy, 40 (2015) 3338-3347 https://doi.org/10.1016/j.ijhydene.2015.01.045.

[48] Eren Şahiner, TL and OSL dose response and stability properties of various commercially glass samples obtained from Turkey for dosimetric purposes in the UV emission spectral region, Applied Radiation and Isotopes, 128 (2017) 68-74 https://doi.org/10.1016/j.apradiso.2017.06.030.

Figures

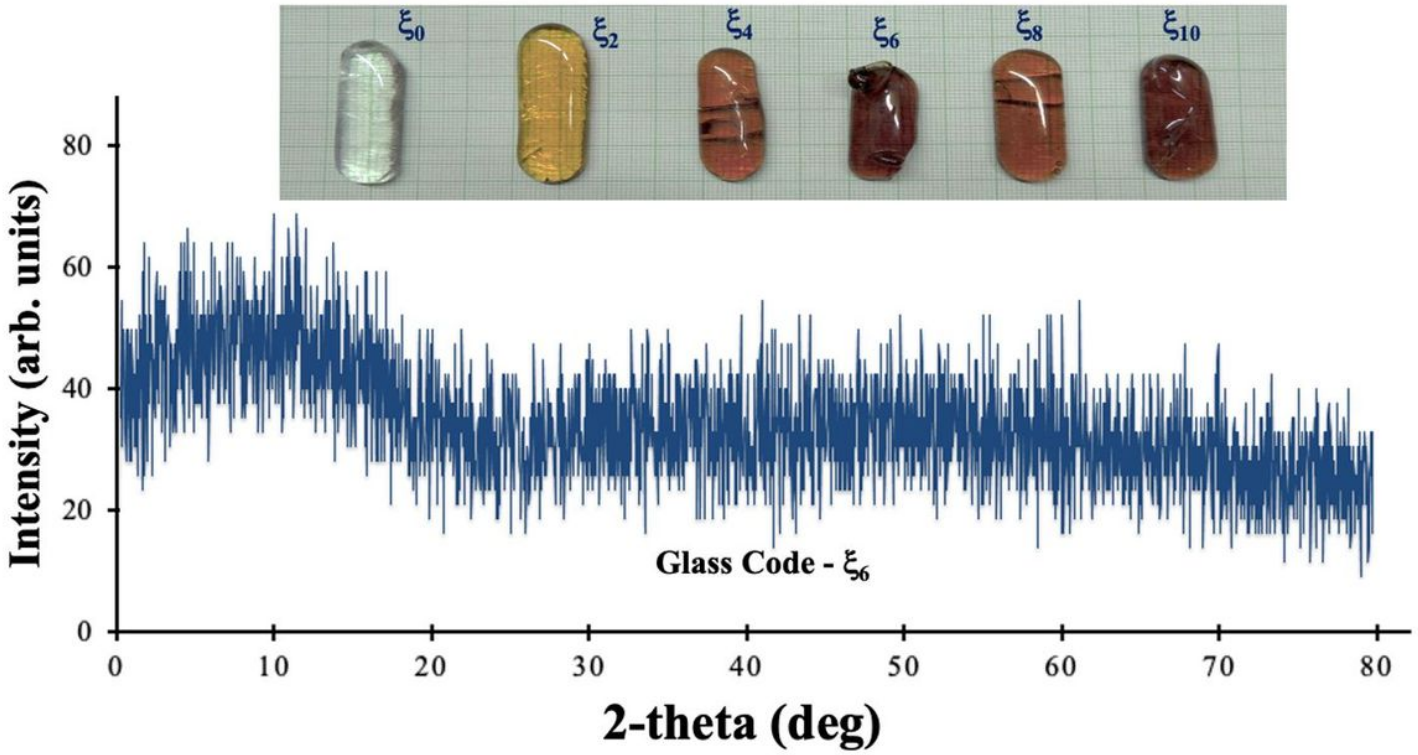

Figure 1

X-Ray diffraction pattern of glass with 0.6 mol% NiO concentration. Inset of the figure represent (10-x)BaO+(x)NiO + 30 La2O3 + 60SiO2 series of glasses. Where ‘x’ varies 0 to 1 mol% with a step size of 0.2 mol%. The diffraction angles are taken up to an accuracy of ± 0.1o. lines drawn back ground of image only for better view of eye guiding.

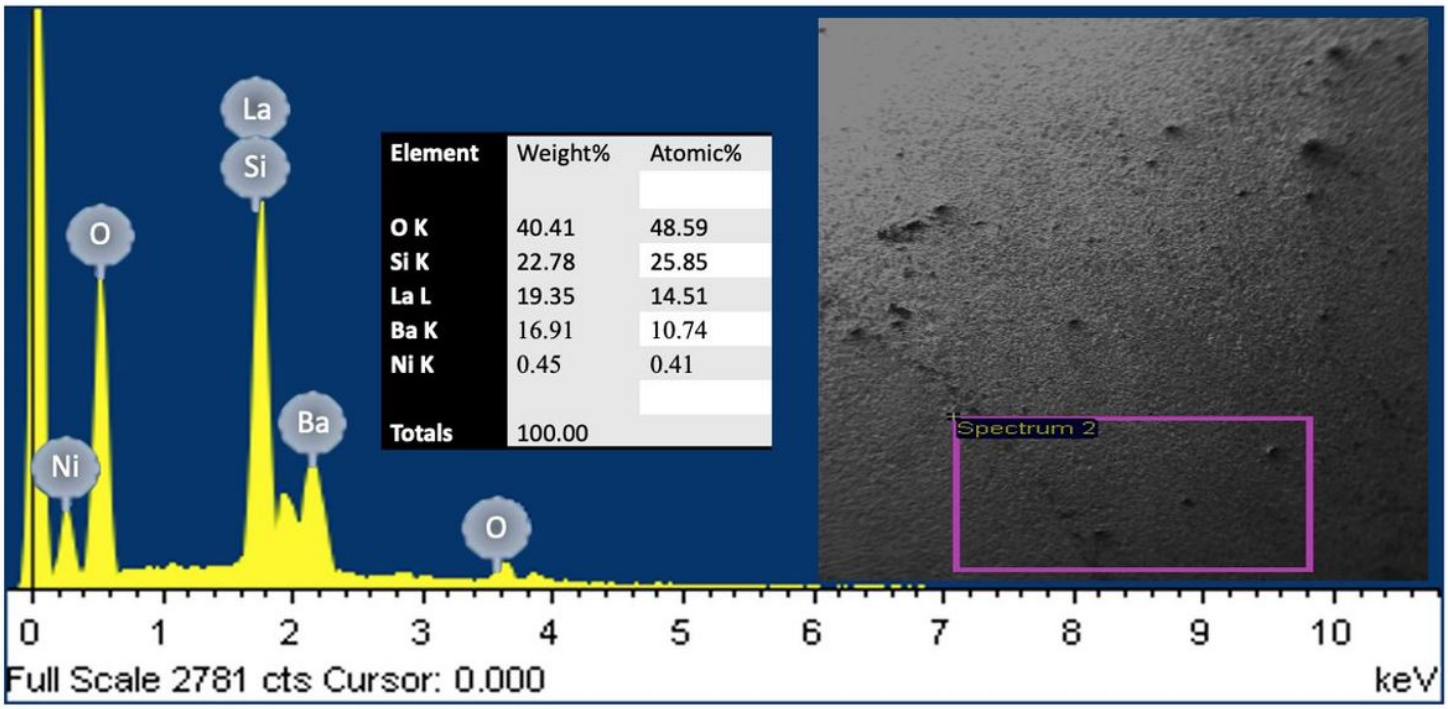

Figure 2

Chemical analysis and surface morphology of ‘ξ6’ glass code (10-x)BaO+(x)NiO+30La2O3+60SiO2 series of glass materials recorded at room temperature with in the energy range of 0-9 keV

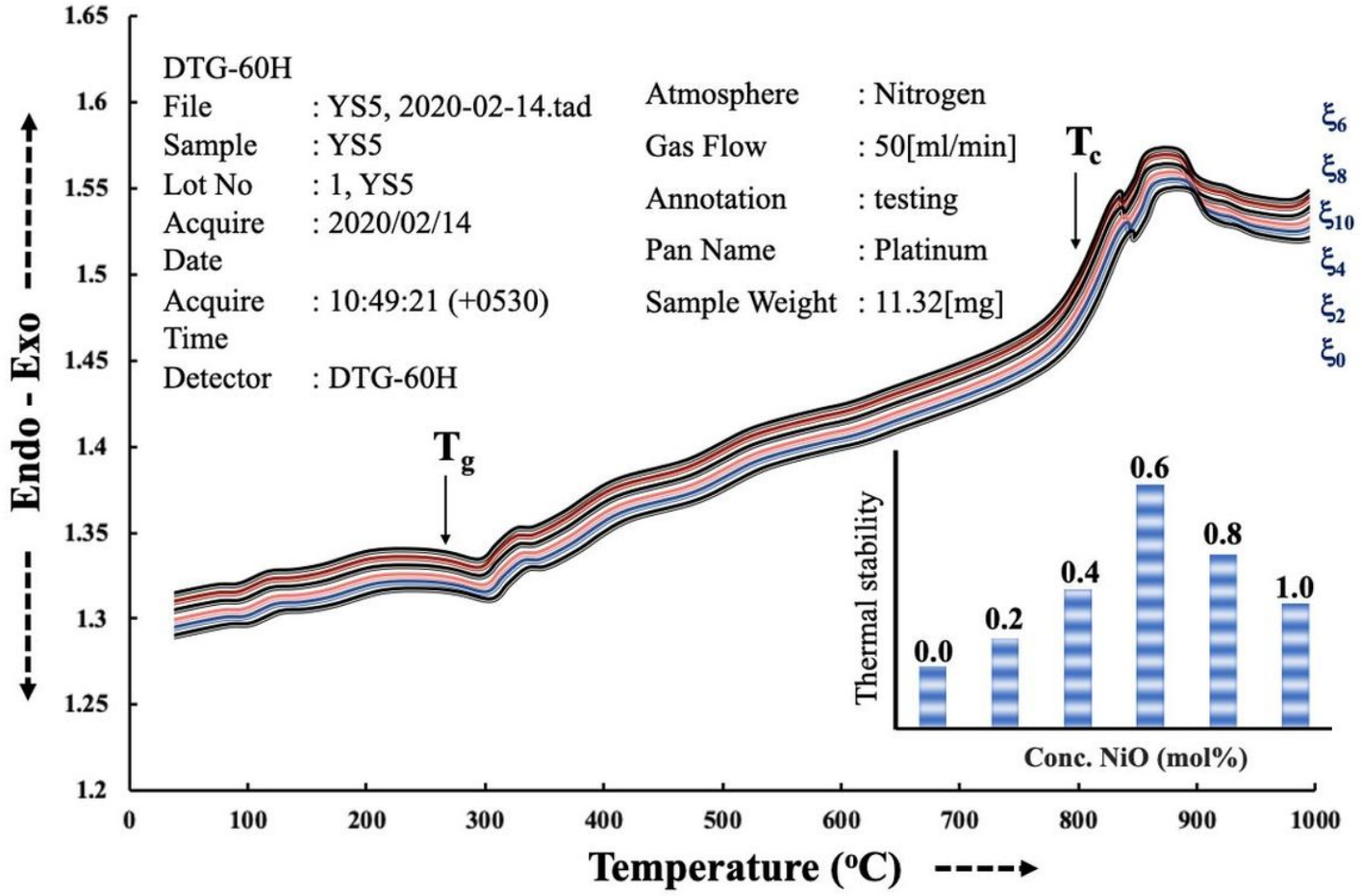

Figure 3

DTA thermograms of ‘ξ6’ glass code of (10-x)BaO +(x)NiO+30La2O3+60SiO2 series of glass materials, where ‘x’ varies 0 to 1 mol% with a step size of 0.2 mol%. Inset (a) shows the variation in thermal stability with increasing concentration of NiO. The temperatures are taken up to an accuracy of ± 1oC and Mac based MATLAB 2.3 version to plot the figure.

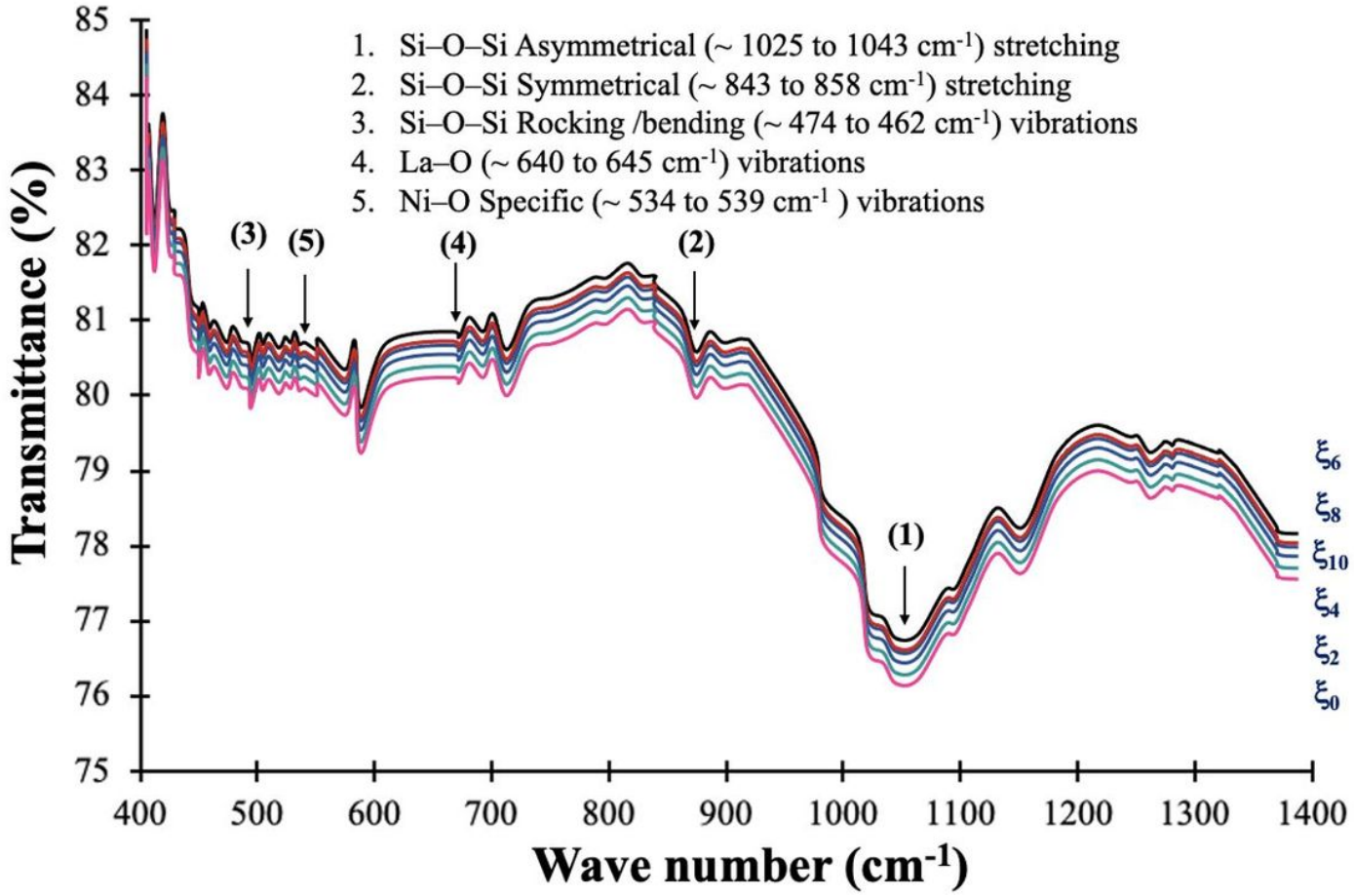

Figure 4

FT-IR spectra of ‘ξ6’ glass code of (10-x)BaO+(x)NiO+30La2O3+60SiO2 series of glass materials recorded at room temperature with in the wave number range of 400 - 1400 cm-1. The wave number are taken up to an accuracy of ± 1 cm-1 and Mac based MATLAB 2.3 version to plot the figure.

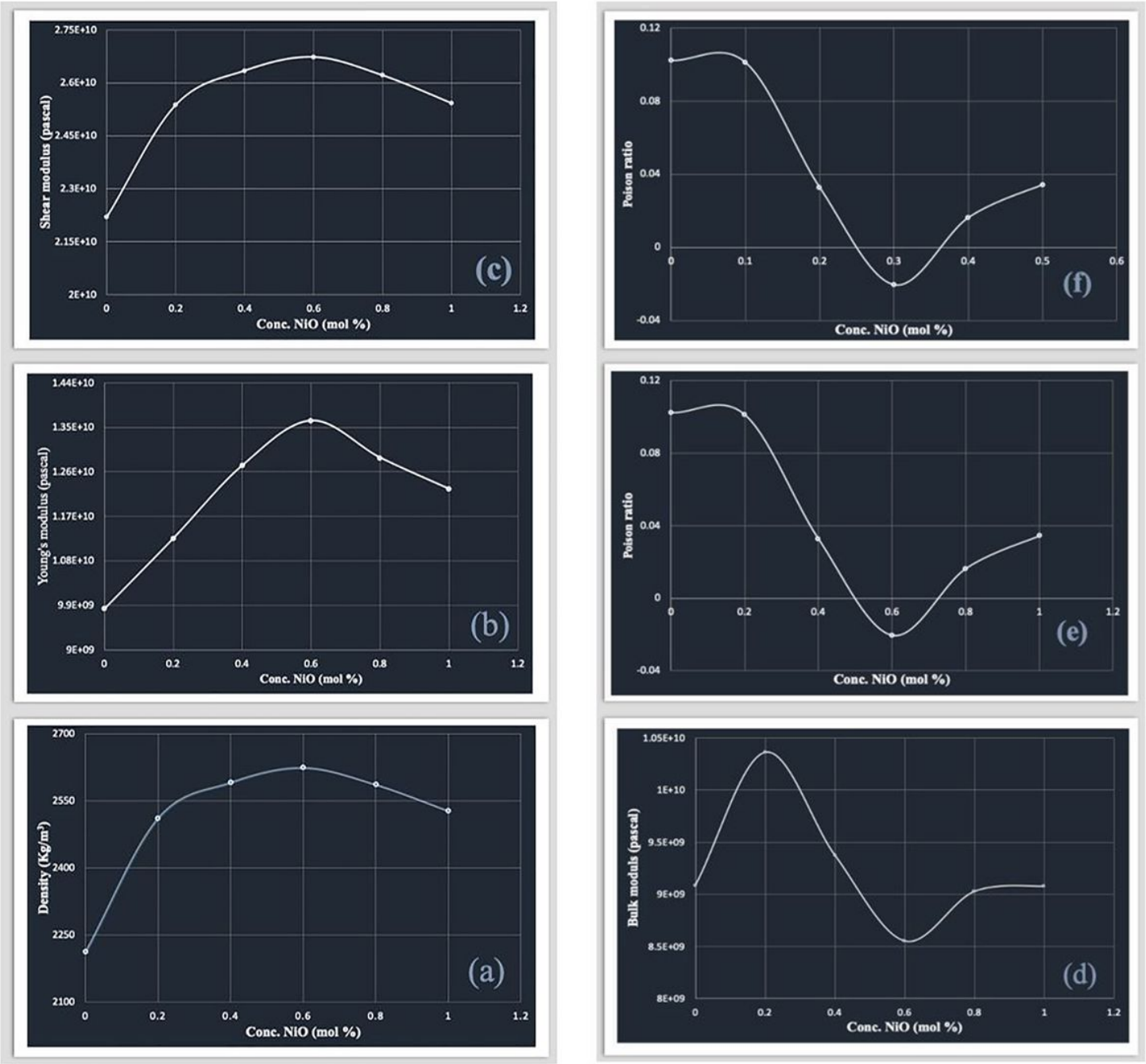

Figure 5

(a) Elastic properties: variation in (a) density, (b) Young's modulus and (c) bulk modulus with NiO concentration (10-x)BaO +(x)NiO+30La2O3+60SiO2 series of glass materials where 'x' varies 0 to 1 mol% with a step size of 0.2 mol%. (b) Elastic properties: variation in (d) shear modulus (e) micro hardness and (f) Poisson ratio with NiO concentration of (10-x)BaO +(x)NiO+30La2O3+60SiO2 series of glass materials where 'x' varies 0 to 1 mol% with a step size of 0.2 mol%.

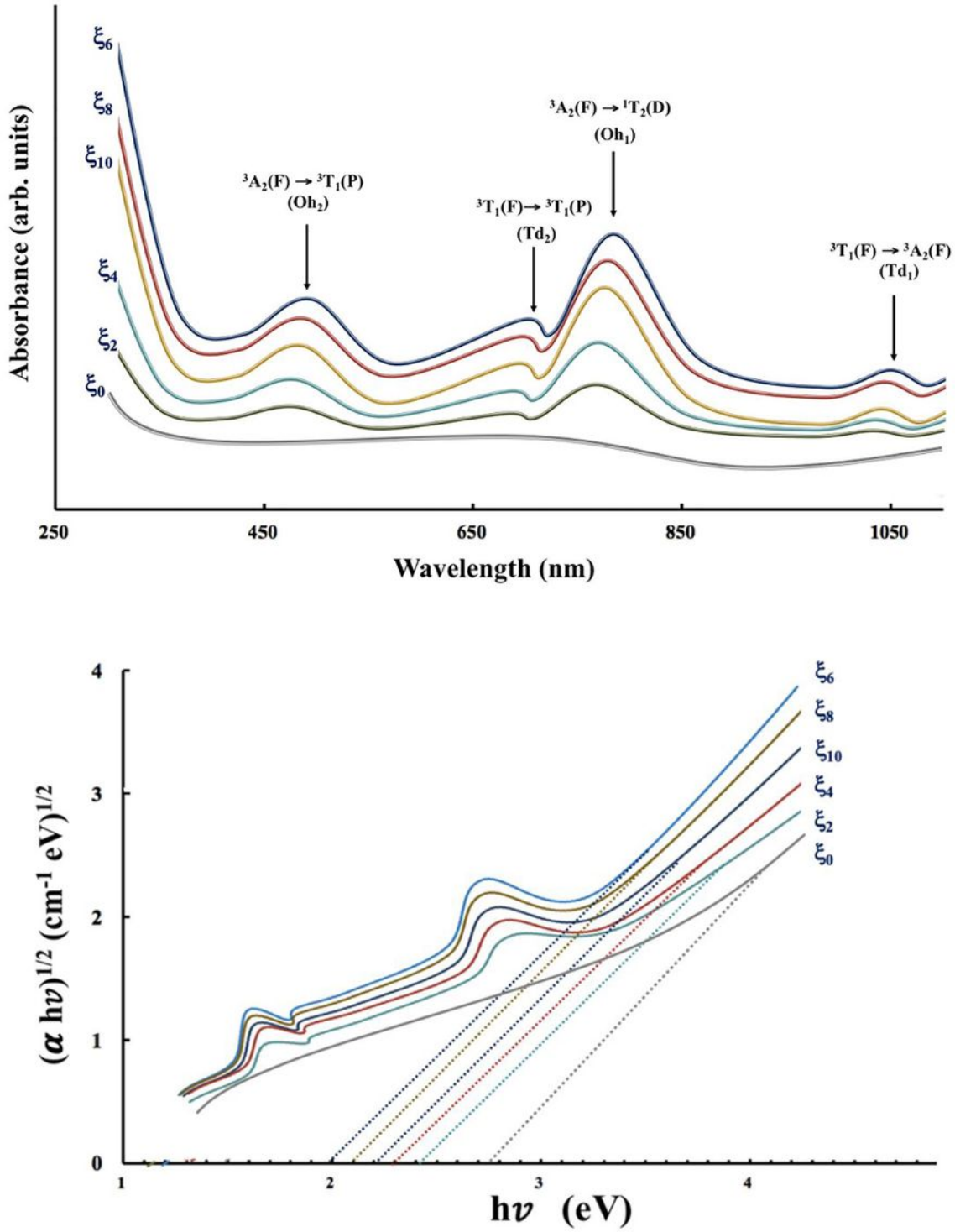

Figure 6

(a) Optical absorption spectra of (10-x)BaO +(x)NiO+30La2O3+60SiO2 series of glass materials recorded at room temperature with in the wavelength range of 200 - 2200 nm range. The wavelengths are taken up to an accuracy of ± 0.1 nm and Mac based MATLAB 2.3 version to plot the figure. (b) Tauc plots of (10-x)BaO +(x)NiO+30La2O3+60SiO2 series of glass materials. Where 'x' varies 0 to 1 mol% with a step size of 0.2 mol%. Wavelengths are taken up to an accuracy of ± 0.1 nm.

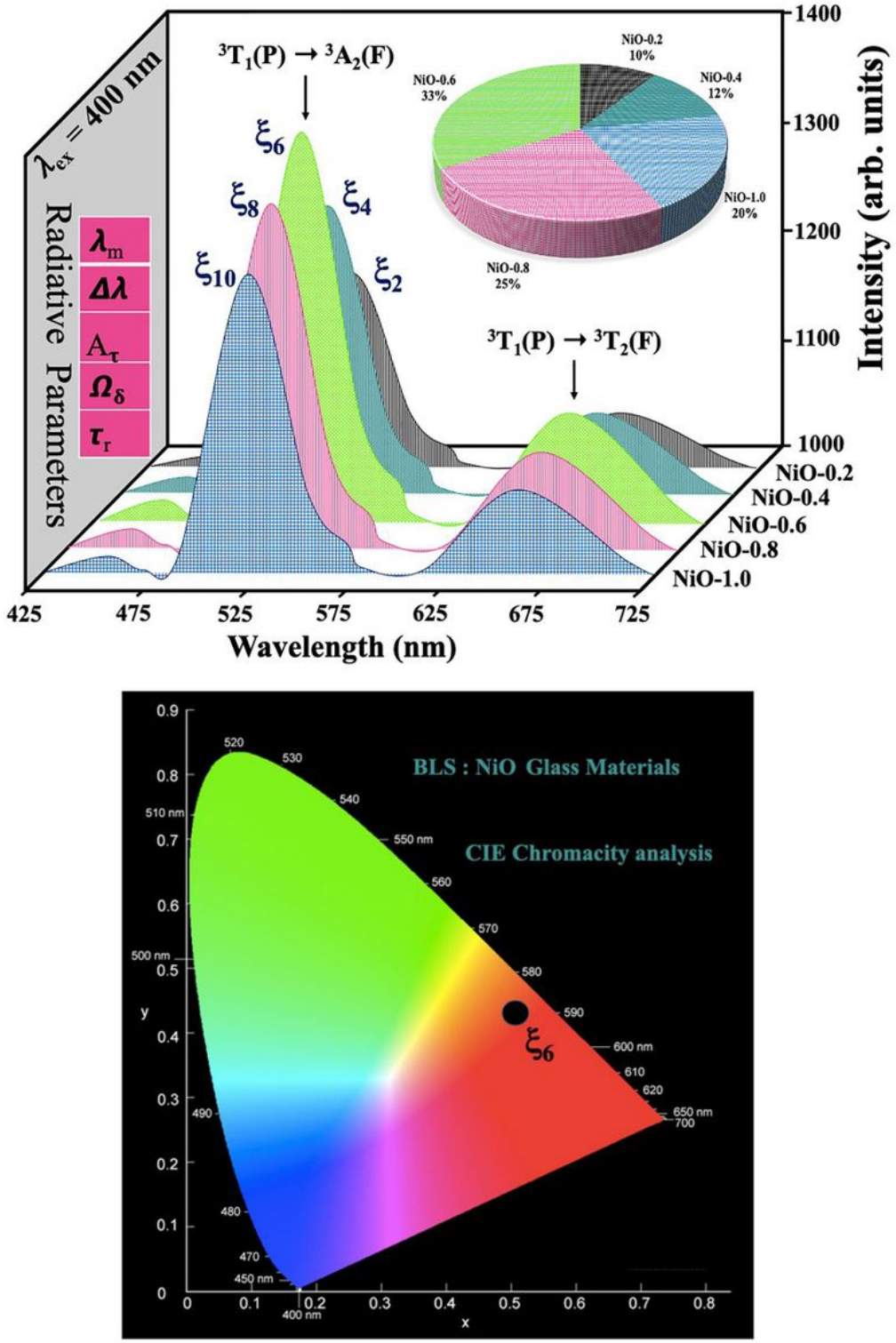

Figure 7

(a) Photoluminescence spectra of (10-x)BaO+(x)NiO+30La2O3+60SiO2 series of glass materials recorded at room temperature with in the wavelength range of 370 to 800 nm and with an excitation wavelengths of both 361 nm. The wavelengths are taken up to an accuracy of ± 0.1 nm and Mac based MATLAB 2.3 version to plot the figure. (b) Chromacity analysis of (10-x)BaO+(x)NiO+30La2O3+60SiO2

series of glass materials, where ‘x’ varies 0 to 1 mol% with a step size of 0.2 mol%. The wavelengths are taken up to an accuracy of ± 0.1 nm and Mac based MATLAB 2.3 version to plot the figure.

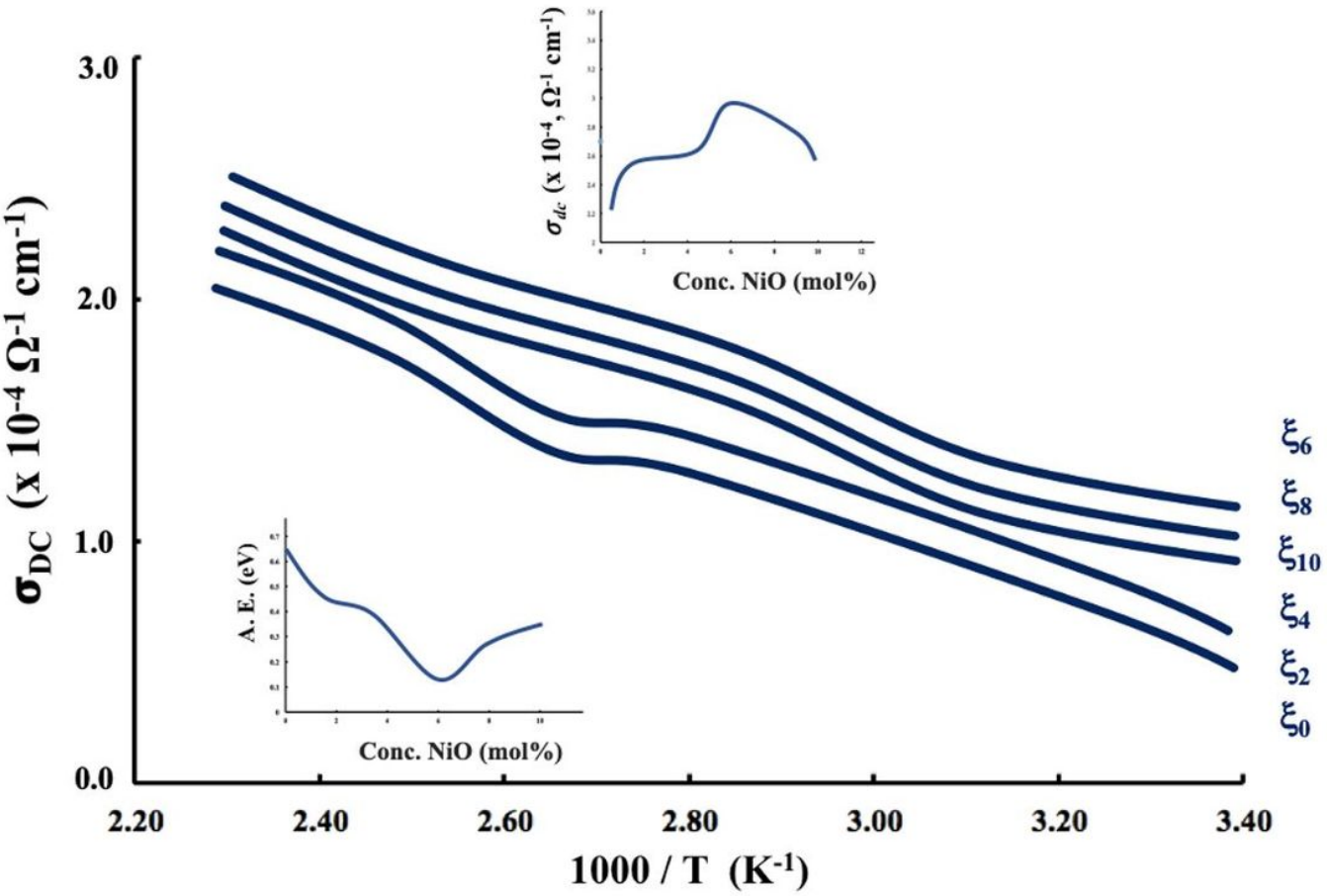

Figure 8

Variation of DC Conductivity with 1/T for (10-x)BaO+(x)NiO+30La2O3+60SiO2 series of glass materials, where ‘x’ varies 0 to 1 mol% with a step size of 0.2 mol%. The inset 8(a) represents variation in activation energy with concentration and inset 8(b) variation in DC conductivity with concentration of NiO. The temperatures are taken up to an accuracy of ± 1oC and Mac based MATLAB 2.3 version to plot the figure.

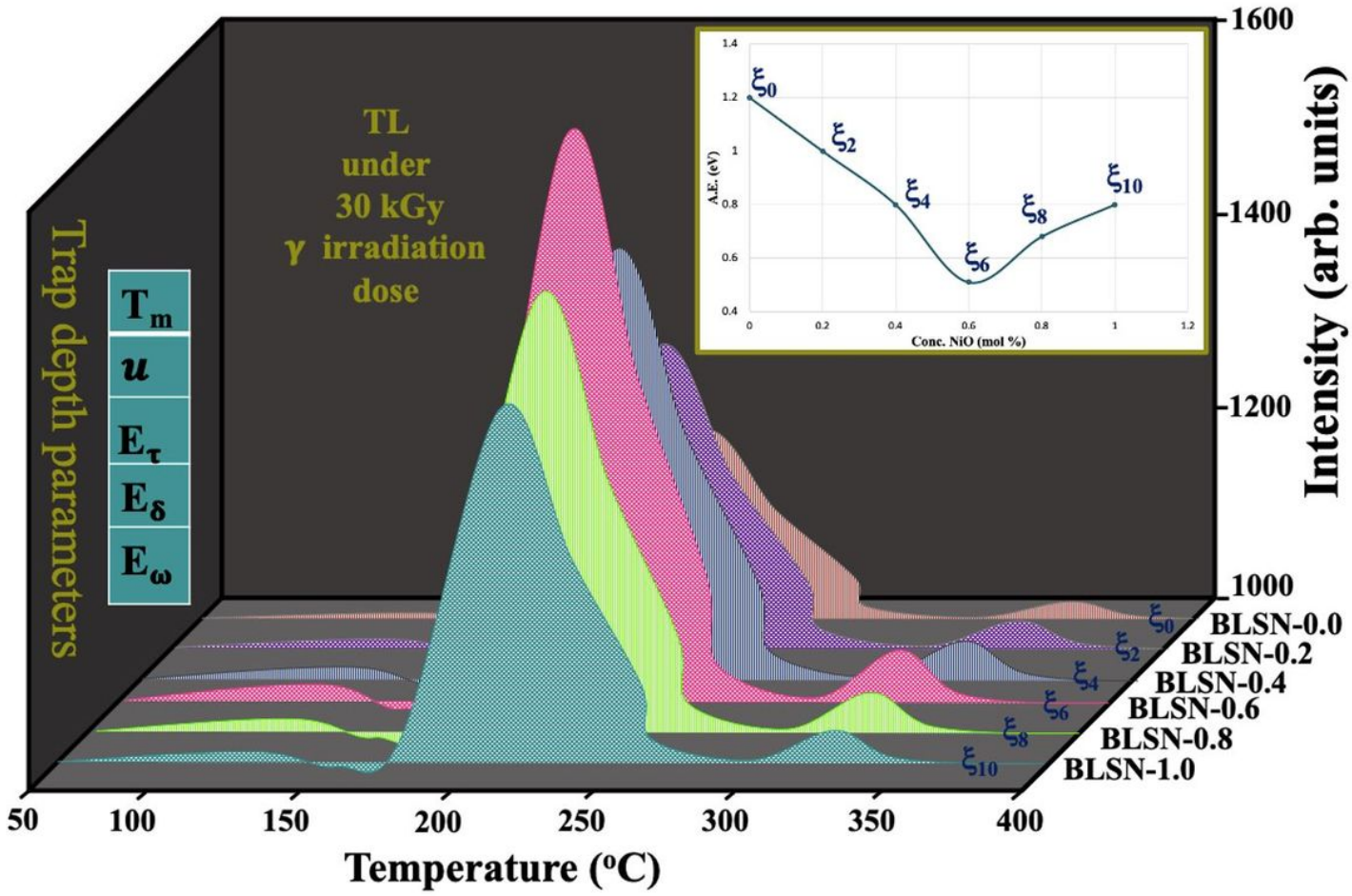

Figure 9

Thermoluminiscence analysis of (10-x)BaO+(x)NiO+30La2O3+60SiO2 series of glass materials, where ‘x’ varies 0 to 1 mol% with a step size of 0.2 mol%. The temperatures are taken up to an accuracy of ± 0.1 oC and Mac based MATLAB 2.3 version to plot the existing figure. Inset of the figure represents variation in A.E. with increasing NiO concentration.

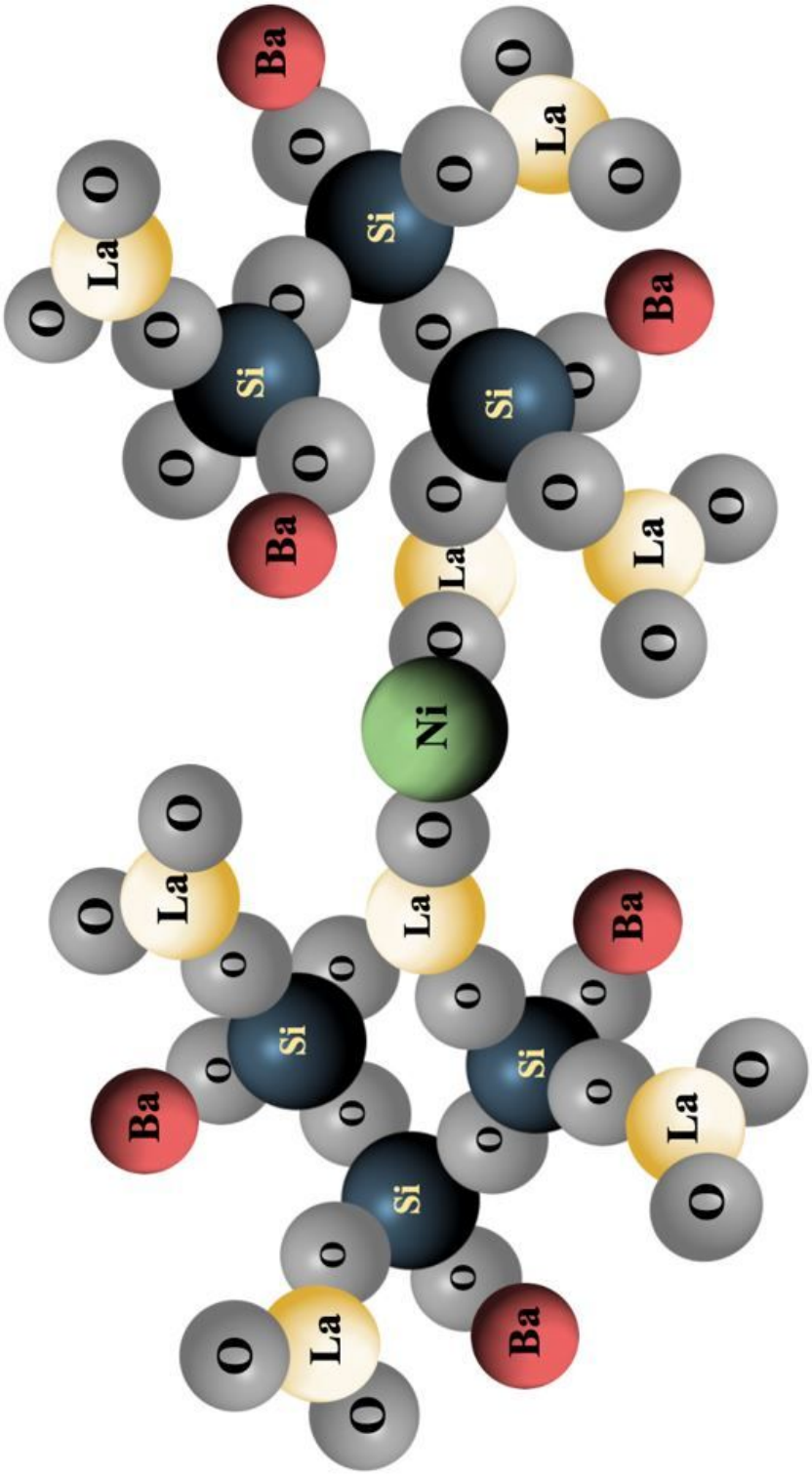

Figure 10

NiO doped alkali lanthanum silicate glass. Mac based Chem Draw Ultra version 12.0 was used to plot the figure.